Int. J. Electrochem. Sci., 12 **(2017)** 280 – 291, doi: 10.20964/2017.01.52

International Journal of
ELECTROCHEMICAL
SCIENCE
www.electrochemsci.org

$CaFe_2O_4$-type Structure $NaRu_2O_4$: a Novel Cathode Material for Li-ion Batteries

Shuqiang Jiao[*], *Pan Zhan, Junxiang Wang*

State Key Laboratory of Advanced Metallurgy, University of Science and Technology Beijing, Beijing, 100083, PR China
[*]E-mail: sjiao@ustb.edu.cn

Received: 7 October 2016 / *Accepted:* 21 November 2016 / *Published:* 12 December 2016

$CaFe_2O_4$-type structure $NaRu_2O_4$ nanorod with a diameter of 100 nm has been synthesized through a simple solid-state method. As a novel cathode material for Li-ion batteries, the nanosized $NaRu_2O_4$ can deliver an initial capacity of 106 mAh g^{-1} at the current density of 20 mA g^{-1} and display a small capacity loss of 0.56% and 0.49% per cycle at the current density of 50 mA g^{-1} and 100 mA g^{-1}. To better understand the process of the Li^+ insertion/extraction, cyclic voltammetry and electrochemical impedance spectroscopy are performed. The $NaRu_2O_4$ nanorod demonstrates a potential of cathode material for Li-ion batteries.

Keywords: Lithium-ion battery; Cathode materials; Sodium ruthenate

1. INTRODUCTION

Energy can be considered as the lifeblood of our modern society. However, the widespread use of fossil fuel doesn't meet the needs of the sustainable development and environment friendly society. So a clean and sustainable energy is essential for the development of human being in the long run. Among all energy storage systems, Lithium-ion batteries (LIBs) are widely considered as the most advanced energy storage systems due to their higher energy conversion efficiencies and energy densities, longer cycle lives and environmental benignity. Nowadays, LIBs are widely used in portable devices such as mobile phones, laptop computers, cameras and so on.[1-5]

However, batteries need to possess a large capacity, an excellent rate capability, and outstanding cycle stability, be safe to meet full demands for the next generation LIBs which are highly desired to use in electronic vehicles and hybrid electronic vehicles. Thus, the search for new electrode materials seems never-ending. The transition metal intercalation oxides have caught the major research

interests as the lithium-ion battery cathodes.[6-12] Categorized by structure, the conventional cathode materials include layered compounds $LiMO_2$ (M=Co, Ni, Mn, etc.), spinel compounds LiM_2O_4 (M=Mn, etc.) and olivine compounds $LiMPO_4$ (M=Fe, Mn, Ni, Co, etc). Most of the researches are performed on these materials and their derivative such as $LiMn_{2-x}Ru_xO_4$,[13] $LiNi_{0.5}Mn_{1.5}O_4$,[14] $LiMMn_{11/6}O_4$ (M=$Co_{1/6}$, $Co_{1/12}Cr_{1/12}$, etc.).[15] Therefore, exploiting other transition metal intercalation oxides of novel electrochemical property as cathode materials for LIBs is still necessary.

$NaRu_2O_4$ crystallizes in the calcium ferrite ($CaFe_2O_4$)-type structure, which is comprised of double chains of edge-sharing RuO_6 octahedra that then share corners with neighboring double chains, creating a zig-zag of RuO_6 dimers. The alkali atom resides in the pseudo-triangular channels created by the corner shared double chains,[16,17] creating a promising tunnel structure for the insertion and extraction of the lithium ions. $NaRu_2O_4$ synthesized with solid-state method shows interesting magnetic property.[16,17] However, there is no report on the feasibility of $NaRu_2O_4$ as cathode material for LIBs. As with other compounds with one-dimensional tunnels,[18-21] the $NaRu_2O_4$ with one-dimensional tunnels may have stable framework and promote the diffusion of the Li^+ in the tunnel. It is suggested meaningful to study the electrochemical properties of $NaRu_2O_4$ as cathode material for LIBs.

In this work, the calcium ferrite ($CaFe_2O_4$)-type $NaRu_2O_4$ was synthesized in a simple solid-state reaction. The process of charging/discharging of the $NaRu_2O_4$ as the cathode material for the LIBs is studied and the electrochemical properties are investigated. It is found that $NaRu_2O_4$ shows excellent cycle performance and moderate rate capability. The present work is also promoting a further exploiting of new materials of the structure type by substitution of ruthenium with other transition metals like Mn, Fe, Ti, etc.

2. EXPERIMENTAL

All materials and chemicals were purchased commercially. $NaRu_2O_4$ was synthesized through a simple solid-state reaction from a mixture of Na_2CO_3 (99.5%, Aladdin) and RuO_2 (99.9%, Aladdin). Both the RuO_2 and the Na_2CO_3 powder were heated to remove absorbed water before use. The RuO_2 powder was heated at 700 ^oC for 2 h, and the Na_2CO_3 powder was heated at 250 ^oC overnight. The reaction mixtures were ground intimately and pressed into a pellet of 10 mm diameter with a 1:2 ratio of Na:Ru. The pellet was heated at 950 ^oC for 12 h under Ar flow.

The crystal structure of the as-prepared material was characterized by X-ray diffraction measurement (XRD, Rigaku, D/max-RB) and the morphology of the as-prepared material was examined by field emission scanning electron microscopy (FESEM, JEOL, JSM-6701F) and transmission electron microscopy (TEM, JEOL, JEM-2010).

The $NaRu_2O_4$ cathode was prepared by mixing 75 *wt*% $NaRu_2O_4$ powder, 15 *wt*% multiwalled carbon nanotubes (MWCNTs) and 10 *wt*% polytetrafluoretyhylene (PTFE) dissolved in ethanol. Then the compounds above were put into an ultrasonic vibration generator to mix uniformly. Finally the mixture was dried at 60 ^oC in an oven to form slurry and then pasted uniformly on Al foil and dried at 120 ^oC for above 12 h. Tablet machine was used to make the electrode smooth and thin enough to

make sure the loading was about 2 mg cm^{-2}. The specific capacity was calculated by the weight of $NaRu_2O_4$ active material. Electrochemical tests of the electrode material were performed with coin cells with the $NaRu_2O_4$ cathode and Li metal as counter and reference electrode. The electrolyte was 1.0 M $LiPF_6$ dissolved in the mixture of ethylene carbonate (EC), dimethyl carbonate (DMC) and ethylmethyl carbonate (EMC) (1:1:1 in volume), and Celgard 2032 microporous membrane as the separator. The cells were assembled in an argon-filled glovebox. The galvanostatic charge/discharge test was conducted at a voltage interval of 1.5 to 4.0 V (*vs.* Li^+/Li) (Neware BTS 5V10mA, Shenzhen). Cyclic voltammetry (CV, CHI 1140A) measurements were performed with a scan rate of 0.1 mV s^{-1} between 1.5 and 4.0 V. Electrochemical impedance spectroscopy (EIS, Princeton P4000) was carried out using perturbation amplitude of 5 mV in an open circuit potential with a frequency range from 100 kHz to 10 mHz.

In order to theoretically investigate the insertion of lithium ions into the $NaRu_2O_4$ structure, the plane-wave pseudopotential method implemented in the CASTEP package was employed. Here, with the lithium ion inserting into the tunnel, the formation energy is defined as:

$$E_f(\mathrm{Li})=[E_{tot}(n\mathrm{Li}+\mathrm{NaRu_2O_4})-E_{tot}(\mathrm{NaRu_2O_4})-nE_{tot}(\mathrm{Li})] \quad (1)$$

Here $E_{tot}(n\mathrm{Li}+\mathrm{NaRu_2O_4})$ is the total energy of the $NaRu_2O_4$ structure containing n lithium ions in a unit cell, $E_{tot}(\mathrm{NaRu_2O_4})$ is the total energy of the $NaRu_2O_4$ structure, and $E_{tot}(\mathrm{Li})$ is the total energy of a lithium atom in the reservoir.

3. RESULTS AND DISCUSSION

$NaRu_2O_4$ is isostructual with $CaFe_2O_4$ and has an orthorhombic lattice structure (*Pnma* space group, the International Centre for Diffraction Data [JCPDS] No.29-1455). The $NaRu_2O_4$ unit cell is made up of double chains of edge-sharing RuO_6 octahedra that share corners with neighboring double chains, creating a zig-zag of RuO_6 dimers. Fig. 1(a) shows the structure of $NaRu_2O_4$, highlighting the pseudo-triangular channels created by the corner shared double chains where the alkali atom resides.[16,17,22] Fig. 1(b) shows the XRD patterns of the as-prepared powders, which is in good agreement with previous results.[17,22] However, the peak positions do match well with the standard card but there is a variation in peak intensity. It is possibly because of the oriented growth of the nanocrystal, presumably along the shortest b-axis.[22]

Fig. 2 shows the SEM and TEM images of the $NaRu_2O_4$ nanorods. As shown in Fig. 2(a), the $NaRu_2O_4$ sample appears to have rod-shaped morphologies. The TEM images of the $NaRu_2O_4$ sample displays rod-like morphology (Fig. 2(b)) and the diameter of the rod-like material synthesized from solid-state method is about 100 nm. However, the surface of the rod looks porous and the inner part is rather dense in TEM. The SEM image shows that the nanorod has a rough surface, which may correspond to the porous surface in the TEM images. The insert selected area electron diffraction (SAED) pattern confirms that the nanorods are single-crystalline structure. The high-resolution TEM image (HRTEM) of the material is shown in Fig. 2(c). The interplanar spacing is about 0.27 nm, which is corresponding to (3 0 2) lattice plane of $NaRu_2O_4$. The lithium ions inserted in the direction of b axis.

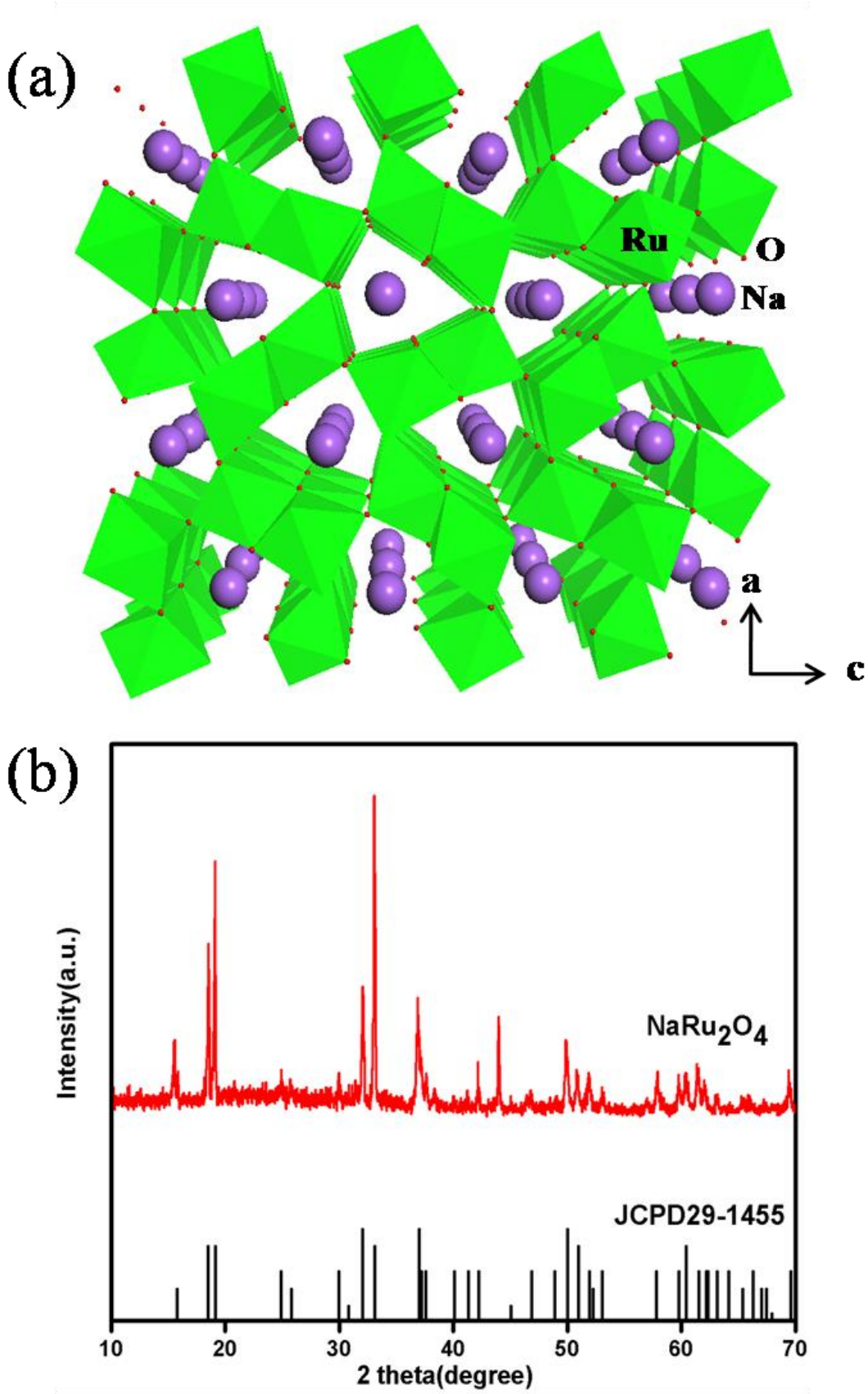

Figure 1. (a) Schematic crystal structure of orthorhombic $NaRu_2O_4$. (b) The XRD patterns of the as-prepared $NaRu_2O_4$.

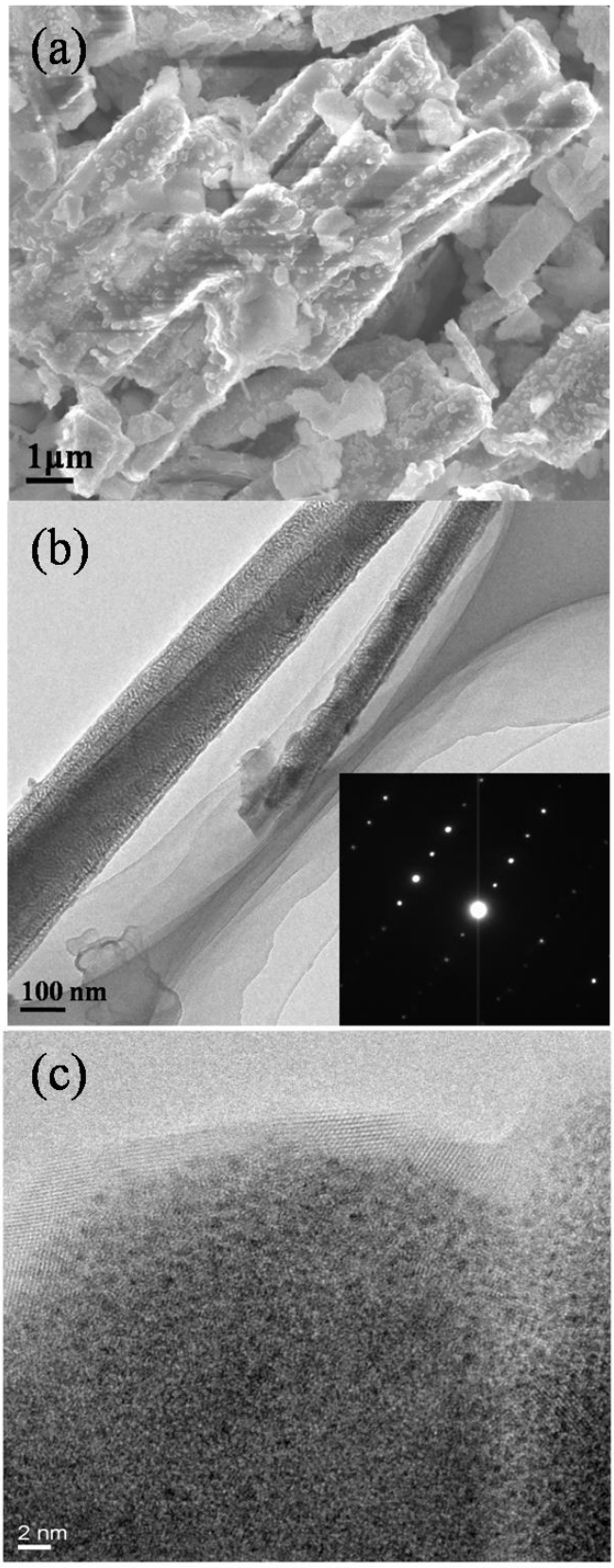

Figure 2. (a) SEM image of the as-prepared $NaRu_2O_4$. (b) TEM image of the $NaRu_2O_4$ nanorods (inset of SAED). (c) High-resolution TEM image of the $NaRu_2O_4$.

Lithium ion insertion/extraction properties of the $NaRu_2O_4$ samples were investigated by cyclic voltammetry (CV) and galvanostatic charge/discharge cycling. Fig. 3 shows typical CV curves of the $NaRu_2O_4$ electrode with a scan rate of 0.1 mV s^{-1} between 1.5 and 4.0 V. It can be observed that two reduction peaks occur at about 2.62 and 3.55 V, which indicates the insertion of lithium ion into the cathode. Simultaneously, two corresponding oxidation peaks locate at 2.65 and 3.75 V, which is associated with the extraction of lithium ions from the cathode. Obviously, the lithium ion insertion/extraction process has two steps and these two redox peaks remain relatively stable during the first three cycles, displaying a good reversibility.

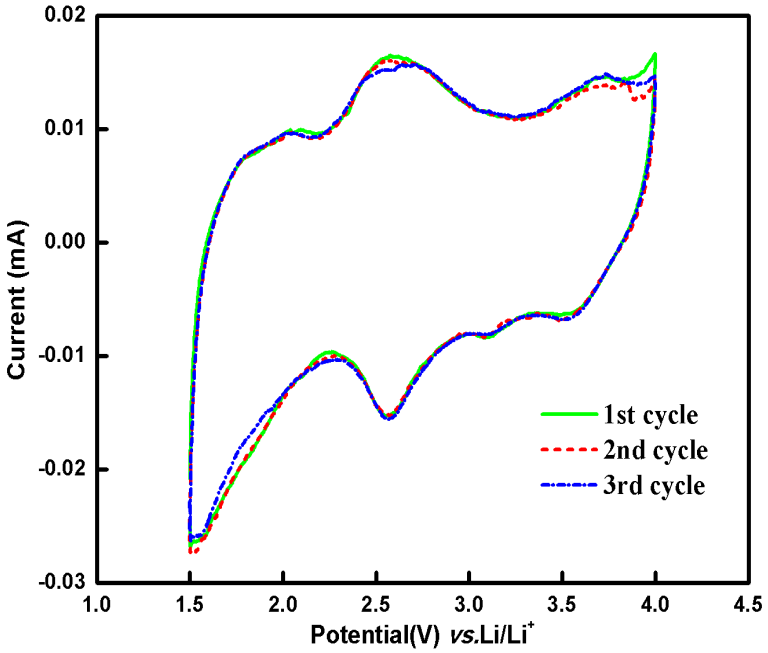

Figure 3. The CV curves of the $NaRu_2O_4$ cathode with a scan rate of 0.1 mV s^{-1} between 1.5 V and 4.0 V in coin-type half-cell.

To clear the theoretical capacity of $NaRu_2O_4$ as cathode material for Li-ion batteries, the plane-wave pseudopotential method implemented in the CASTEP package was employed to investigate the insertion of lithium into the $NaRu_2O_4$ structure. Fig. 4(a) presents the formation energy calculated by the first-principles theory with respect to the number of lithium ions in a $NaRu_2O_4$ unit cell. The more negative of the formation energy, the more stable the lithium ions located in the lattice. As we can see in Fig. 4(a), the more Li ions inserts, the more negative formation energy is observed, indicting the structure is more stable. The detailed first-principles geometry analysis is showing in Fig. 4(b). It can be seen that the volume of the $NaRu_2O_4$ cell does not change over 2 $Å^3$ until more than one Li ions insert into the bulk of the material (10 $Å^3$ with 1.25 Li ions insertion). The tunnel collapses immediately when 1.25 Li ions insert into the tunnel, as a result of which, only one Li ion can be inserted/extracted in the bulk of $NaRu_2O_4$. The theoretical capacity of the $NaRu_2O_4$ is calculated to be 92.7 mAh g^{-1} in terms of the first-principles simulations.

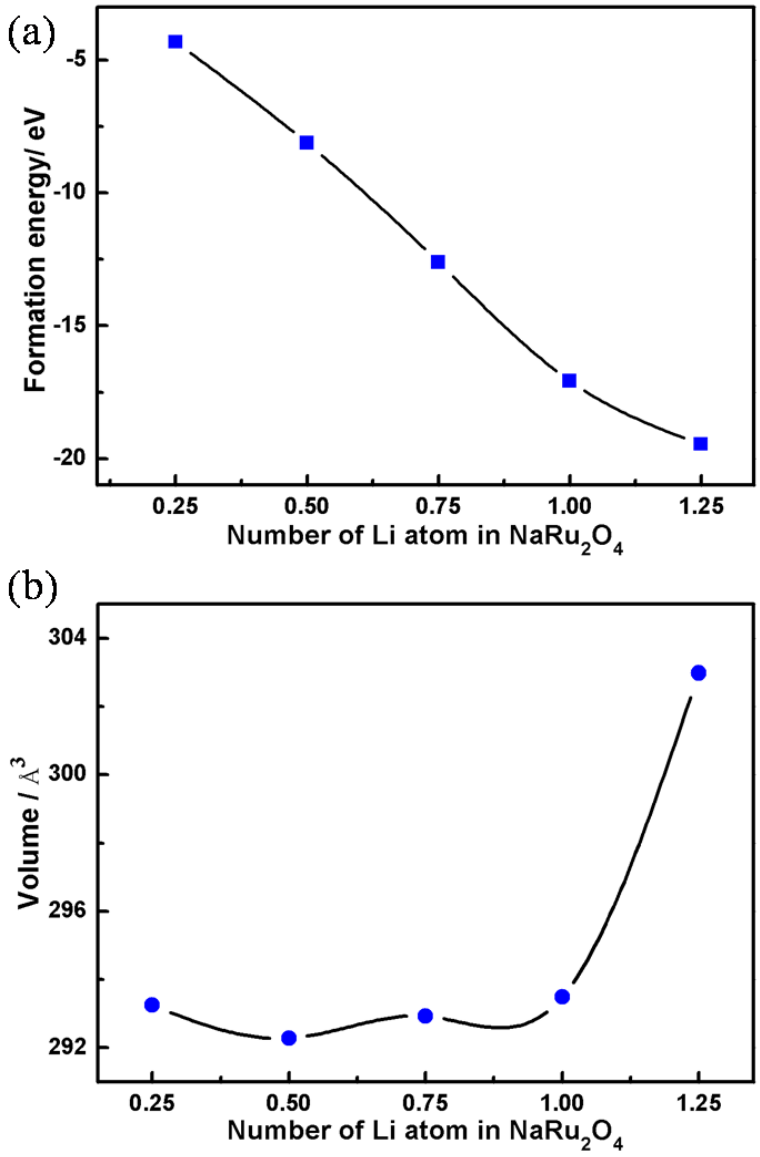

Figure 4. (a) Calculated formation energy of lithium as a function of its number in $NaRu_2O_4$ unit cell. (b) The unit cell volume with respect to the number of Li ions in the bulk of $NaRu_2O_4$.

In order to display the high cycling performance of the $NaRu_2O_4$ cathode, the charge-discharge cycling performance of the as-prepared cathode was carried out between 1.5 and 4.0 V under different current densities. Fig. 5 shows the initial charge-discharge curves of the cathode at the charge/discharge current density of 20, 50 and 100 mA g^{-1}. The voltage plateaus at all rates are consistent with the CV curve profiles. The initial charging capacities are about 10 mAh g^{-1} higher than the initial discharging capacities, indicating some degree of irreversible reactions, which is attributed to some side reactions such as the decomposition of the electrolyte.[23] The initial specific discharge capacities of the cathodes are 106, 90.8 and 63.8 mAh g^{-1} at the current density of 20, 50 and 100 mA g^{-1}, showing capacity retention of 85.7% and 60.2% compared with the capacity at the current density of 20 mA g^{-1}. Therefore, the $NaRu_2O_4$ cathode demonstrated a restrictive electrochemical capacity at the high rate.

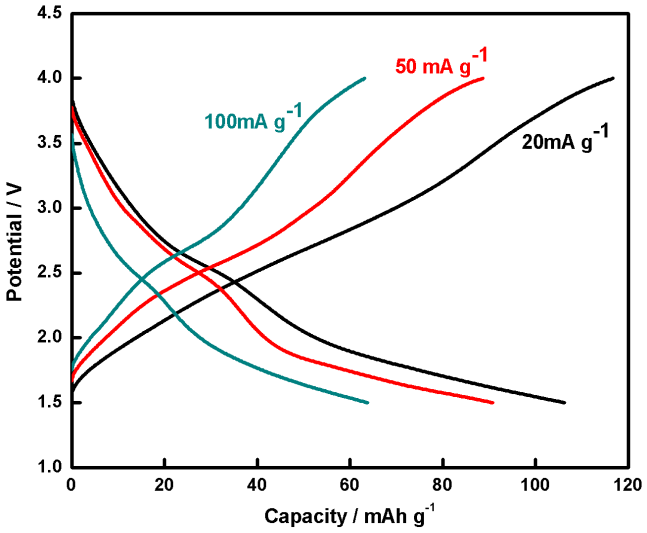

Figure 5. Initial charge and discharge curves of $NaRu_2O_4$ at the current density of 20mA g^{-1}, 50mA g^{-1} and 100mA g^{-1}, respectively.

Fig. 6 illustrates the cycle performance at the charge/discharge current density of 20, 50 and 100 mA g^{-1}. The results show that the specific capacity gradually decreases with the increase of the charge/discharge rate.

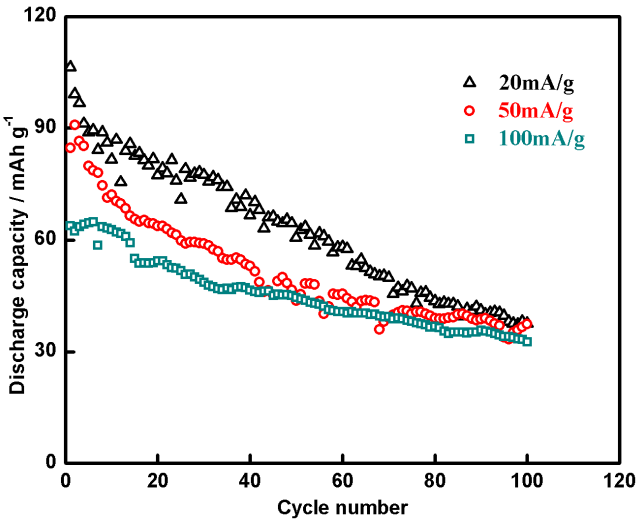

Figure 6. Specific discharge capacity tested at different current densities over 100 cycles

However, the specific capacity fades much faster at the current density of 20 mA g^{-1} than that of other two current densities, reaching capacity retention of only 35.3% after 100 cycles. We attribute this phenomenon to that when cycled at such a low rate, the charge and discharge depth is more extensive, which may bring about a collapse of the crystallographic structure of this material. In order to confirm that, TEM images with the SAED pattern of the 5 cycled and 100 cycled electrode at 20 mA g^{-1} have been provided in Fig 7. The single-crystalline structure in Fig. 2(b) gradually transformed

into a small part of polycrystalline structure (Fig. 7(a)) and finally polycrystalline structure (Fig. 7(b)). In contrast, the cell cycled at the current density of 50 mA g^{-1} and 100 mA g^{-1} still displayed a discharge capacity of 37.5 mAh g^{-1} and 32.7 mAh g^{-1} after 100 cycles, corresponding to 44.2% and 51.2% capacity retention compared with the capacity of the first cycle. The capacity loss of the sample mainly occurring in the first few cycles (29.8% and 15.2% capacity loss during the first 20 cycles), as a result of which, the $NaRu_2O_4$ have an excellent cycle performance at the rate of 50 mA g^{-1} and 100 mA g^{-1}.

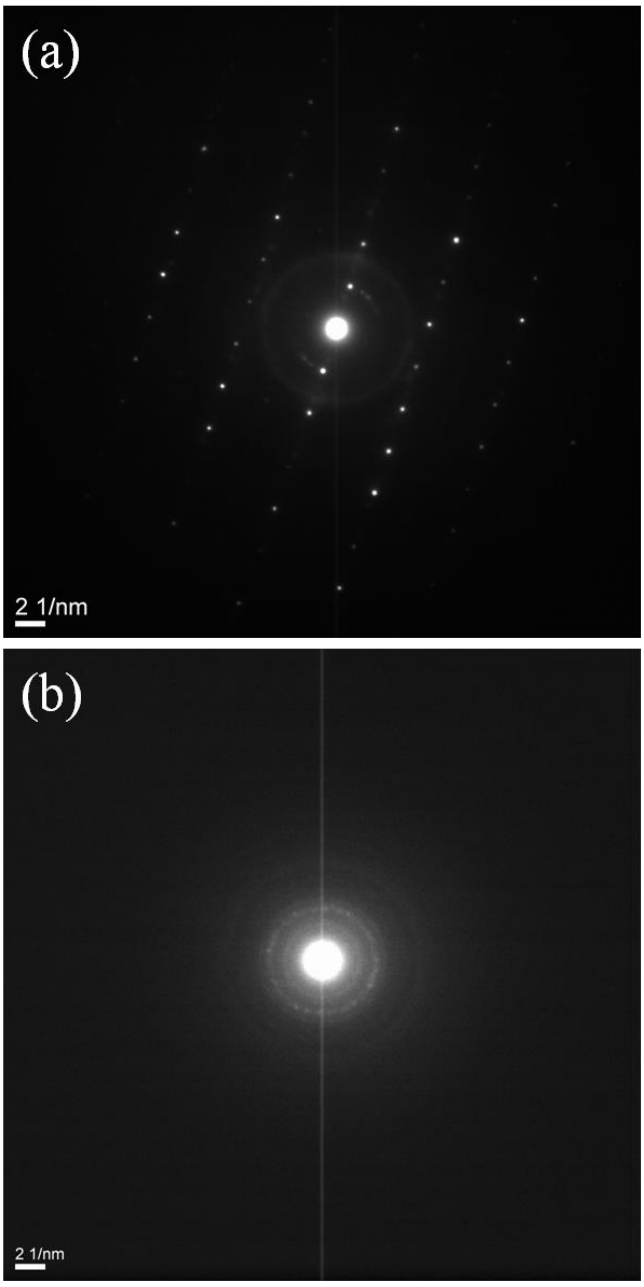

Figure 7. The SAED patterns of (a) 5 cycled electrode and (b) 100 cycled electrode at 20 mA g^{-1}

EIS is one of the most informative analytical techniques that can be employed to understand reaction kinetics of the Li-ion insertion/deinsertion process in compounds due to its nondestructive

nature and ability to differentiate various phenomena taking place in an electrode at different time periods.[24] To further understand the electrochemical behavior of the $NaRu_2O_4$ electrode, EIS measurements of batteries cycled at different current densities were carried out at a frequency range from 100 kHz to 10 mHz. The Nyquist plot of the $NaRu_2O_4$ composite cathodes of the fresh cell and cycled cell are presented in Fig. 8. As shown in Fig. 8, in the low frequency region, an inclined line is mainly attributed to the semi-infinite diffusion of Li ions into the bulk of the $NaRu_2O_4$ composites, which is the Warburg diffusion. In the high frequency region, it can be seen that the cathode displays one depressed semicircle, which is indicative of the charge transfer resistance (R_{ct}) of Li-ion intercalation by a faradic process. The charge transfer resistance of the fresh battery corresponding to the diameter of the semicircle remains at a low level, and the R_{ct} remains the same after 100 cycles at the current density of 50 mA g^{-1}, showing a good performance at moderate current density. However, the R_{ct} of the cells cycled at the current densities of 20 mA g^{-1} and 100 mA g^{-1} almost doubled, indicating some degree of structure collapse of the structure under extensive charge and discharge conditions which is consist of Fig. 7. So the high rate charging/discharging process of the $NaRu_2O_4$ cathode are controlled by the diffusion of the Li ions in the bulk of the material, which agrees with Fig. 5. Therefore, to further enhance the rate performance of $NaRu_2O_4$ with the methods such as doping and optimization of particle size.

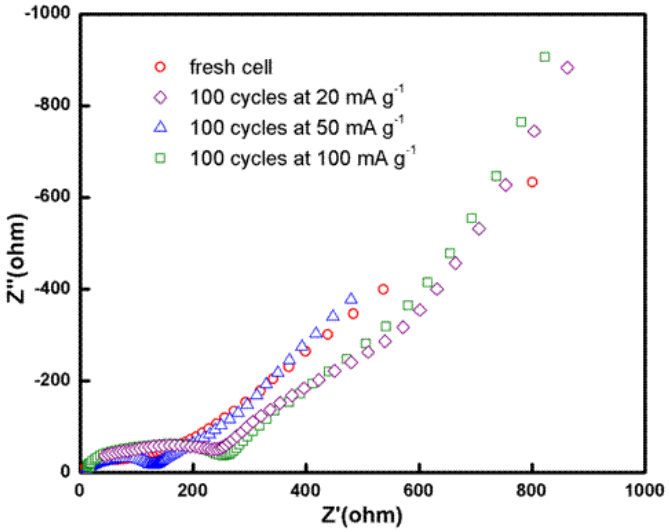

Figure 8. Nyqusit plots of the $NaRu_2O_4$ composite fresh cathode and cycled cells at 20, 50, and 100 mA g^{-1} in an open-circuit potential with a frequency range from 100 kHz to 10 mHz.

The rate capability of the $NaRu_2O_4$ cathode was tested at various current densities of 20, 50, 100 and 20 mA g^{-1}, as shown in Fig. 9. It can be observed that the reversible capacity of the electrode decays at the first twenty cycles to 81.8 mAh g^{-1}, and remains at about 55.7 mAh g^{-1} at 50 mA g^{-1}, 45.4 mAh g^{-1} at 100 mA g^{-1}. The $NaRu_2O_4$ cathode reveals extraordinary performance at the high rate. Even when the current density returns to 20 mA g^{-1} after cycling at the high current density of 100 mA g^{-1}, the reversible capacity can be maintained at 71.6 mAh g^{-1}, showing an excellent cyclic performance. The reversible capacity of the nanorod $NaRu_2O_4$ electrode at 20 mA g^{-1} is actually about 15 mAh g^{-1}

higher than the theoretical capacity of $NaRu_2O_4$. In this material, one lithium ion can be inserted and extracted during the cycling. The slightly higher than theoretical capacity suggests some degree of pseudocapacitor performance which is also revealed by that no obvious charge-discharge plateau can be seen in the charge/discharge curves. In addition to that, the rough surface of material is also beneficial to the pseudocapacitor performance. Indeed, the fast and reversible redox process on the surface of the activated materials, in combination with the formation of electric double layer or Faradaic reactions, allows the pseudocapacitor to store energy.[25,26]

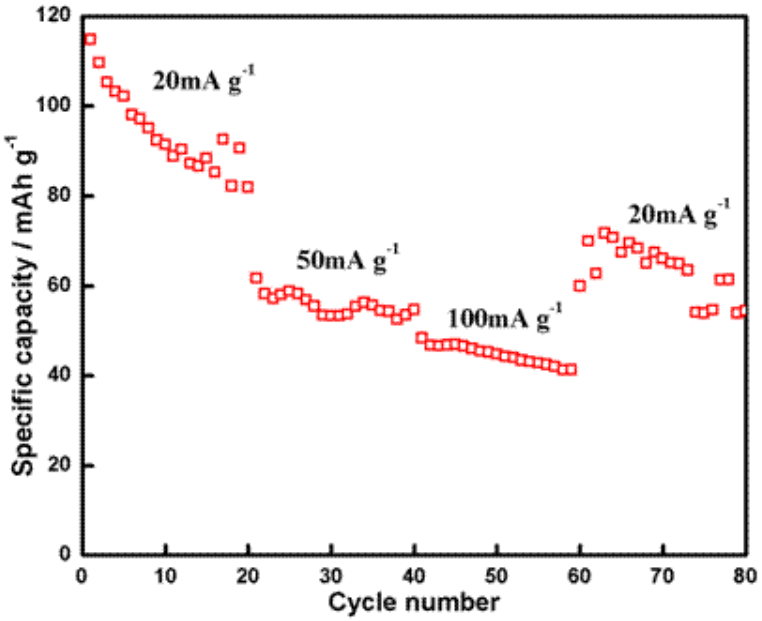

Figure 9. Discharge capacity of the $NaRu_2O_4$ as a function of charge/discharge cycles at different current densities of 20, 50, 100, and 20 mAh g^{-1}.

4. CONCLUSION

$NaRu_2O_4$ was successfully synthesized through a simple solid-state method. The FESEM and TEM images show that the crystal grew with a long bar-shape along the shortest b-axis. The CV curve shows that the lithium ion extraction/insertion process had two steps and the cathode displayed a good reversibility. The initial charge progress accompanies some degree of the decomposition of electrolyte. It could be observed that the $NaRu_2O_4$ cathode display an initial discharge capacity of 106 mAh g^{-1} at the current density of 20mA g^{-1} and hold capacity retention of 85.7% and 60.2% at the current density of 50 and 100 mAh g^{-1}. It demonstrates a small capacity loss of 0.56% and 0.49% per cycle at the current density of 50 and 100 mA g^{-1}, showing good cycle stability. Because of the severe polarization at the high rate, the $NaRu_2O_4$ cathode has moderate rate ability. Based on the strategies used to improve the performance of other electrodes, it is found that solution to enhance the rate capacity of the $NaRu_2O_4$ cathode may be doping and optimization of particle size.

ACKNOWLEDGEMENT
This work was supported by the Fundamental Research Funds for the Central Universities (FRF-TP-15-002C1).

References

1. B. Scrosati, and J. Garche, *J. Power Sources*, 195(2010)2419.
2. J.M. Tarascon, N. Recham, M. Armand, N. Chotard, P. Barpanda, W. Walker, and L. Dupont, *Chem. Mater.*, 22(2009)724.
3. T. Stephenson, Z. Li, B. Olsen and D. Mitlin. *Energ Environ Sci*, 7 (2014) 209.
4. Z. Yang, D. Choi, S. Kerisit, K.M. Rosso, D. Wang, J. Zhang, G. Graff, and J. Liu, *J. Power Sources*, 192(2009)588.
5. V. Etacheri, R. Marom, R. Elazari, G. Salitra, and D. Aurbach, *Energy Environ. Sci*., 4(2011) 3243.
6. M.V. Reddy, G.V. Subba Rao, and B.V.R. Chowdari, *Chem. Rev*., 113(2013)5364.
7. M.S. Whittingham, *Chem. Rev.*, 104(2004)4271.
8. S. Huang, B. E. Wilson, W. H. Smyrl, D. G. Truhlar and A. Stein. *Chemi Mater*, 28 (2016) 746
9. J.M. Tarascon, and M. Armand, *Nature*, 414(2001)359.
10. W. Liu, P. Oh, X. Liu, M. Lee, W. Cho, S. Chae and J. Cho, *Angew Chen int Edit*, 54, (2015)4440.
11. Y.Y. Xia, and M. Yoshio, *J. Electrochem. Soc.*, 143(1996)825.
12. Y. Zhao, C. Han, J. Yang, J. Su, X. Xu, S. Li and B. Song. *Nano lett*, 15 (2015) 2180.
13. M.V. Reddy, S.S. Manoharan, J. John, B. Singh, G.V. Subba Rao, and B.V.R. Chowdari, *J. Electrochem. Soc.*, 156(2009)A652.
14. M.V. Reddy, H.Y. Cheng, J.H. Tham, C.Y. Yuan, H.L. Goh, and B.V.R. Chowdari, *Electrochim. Acta*, 62(2012)269.
15. T. F. Yi, W. Tao, B. Chen, Y. R. Zhu, S. Y. Yang and Y. Xie. *Electrochimic. Acta*, 188 (2016)686.
16. R.V. Panin, N.R. Khasanova, A.M. Abakumov, W. Schnelle, J. Hadermann, and E.V. Antipov, *Russ. Chem. Bull.*, 55(2006)1717.
17. K.A. Regan, Q. Huang, M. Lee, A.P. Ramirez, and R.J. Cava, *J. Solid State Chem.*, 179 (2006) 195.
18. A.K. Padhi, K.S. Nanjundaswamy, and J.B. Goodenough, *J. Electrochem. Soc.*, 144 (1997)1188.
19. M.M. Thackeray, *Prog. Solid State Chem.*, 25(1997) 1.
20. L.D. Noailles, C.S. Johnson, J.T. Vaughey, M.M. Thackeray, *J. Power Sources*, 81 (1999)259.
21. N. Sharma, J. Plevert, G.V.S. Rao, B.V.R. Chowdari, T.J. White, *Chem. Mater.*, 17 (2005)4700.
22. Y.H. Jung, D.K. Kim, and S.T. Hong, *J. Power Sources*, 233(2013) 285.
23. P. Verma, P. Maire, and P. Novák, *Electrochim. Acta*, 55(2010)6233.
24. M.V. Reddy, B.L.W. Wen, K.P. Loh, and B.V.R. Chowdari, *ACS appl. Mater. Interfaces*, 5 (2013)7777.
25. J. Kang, S.H. Wei, K. Zhu, and Y.H. Kim, *J. Phys. Chem. C*, 115(2011)4909.
26. N. Mahmood, M. Tahir, A. Mahmood, J. Zhu, C. Cao and Y. Hou. *Nano Energy*, 11 (2015)267.